

Supporting Information for

Achieving High Room-Temperature Thermoelectric Performance in Cubic AgCuTe

Jing Jiang^{1,2,#}, Hangtian Zhu^{2,#}, Yi Niu^{1,#}, Qing Zhu², Shaowei Song², Ting Zhou^{1,2}, Chao

Wang^{1,*}, Zhifeng Ren^{2,*}

¹Clean Energy Materials and Engineering Center, State Key Laboratory of Electronic Thin Film and Integrated Device, School of Electronic Science and Engineering, University of Electronic Science and Technology of China, Chengdu 611731, China

²Department of Physics and TcSUH, University of Houston, Houston, Texas 77204, USA

*E-mail: cwang@uestc.edu.cn; zren@uh.edu

#These authors contributed equally to this work

This supporting information includes:

Fig.S1 Temperature dependence of thermoelectric properties for AgCuTe and AgCuTe_{0.9}Se_{0.1}.

Fig.S2 Room-temperature XRD analyses for the AgCuTe_{1-z}Se_z (z=0.05, 0.1, 0.12, 0.2, 0.25) samples.

Fig.S3 Room-temperature XRD analyses for the Ag_yCu_{2-y}Te_{0.9}Se_{0.1} (y=0.6, 0.8, 0.9, 1, 1.2, 1.4) samples.

Fig.S4 Temperature-dependent XRD analyses for the (AgCu)_{0.995}Te_{0.9}Se_{0.1} sample.

Fig.S5 The SAED pattern of the main phase with the electron beam along the direction of [1-10] and [111].

Fig.S6 Microstructure analyses of the FCC phase for the AgCuTe_{0.9}Se_{0.1} sample.

Fig.S7 Room-temperature XRD analyses for the AgCuTe_{0.9}Se_{0.1} sample after high-temperature measurements and long-term annealing.

Fig.S8 Room-temperature SEM analyses for the (AgCu)_{0.995}Te_{0.9}Se_{0.1} sample with a hot-press temperature of 473K.

Fig.S9 Room-temperature SEM image with the EDS mapping results for the (AgCu)_{0.995}Te_{0.9}Se_{0.1} sample with a hot-press temperature of 473K.

Fig.S10 Room-temperature SEM analyses for the $(\text{AgCu})_{0.995}\text{Te}_{0.9}\text{Se}_{0.1}$ sample with a hot-press temperature of 923K.

Fig.S11 Fake ultra-high ZT s for the $(\text{AgCu})_{0.995}\text{Te}_{0.9}\text{Se}_{0.1}$ sample with a hot-press temperature of 923K.

Fig.S12 Room-temperature SEM analysis for the $(\text{AgCu})_{0.995}\text{Te}_{0.9}\text{Se}_{0.1}$ sample with a hot-press temperature of 823K.

Fig.S13 Room-temperature XRD analysis for the $(\text{AgCu})_{0.925}\text{Te}_{0.9}\text{Se}_{0.1}$ sample.

Fig.S14 Low-temperature (300 K-373 K) stability of thermoelectric properties in $(\text{AgCu})_{0.995}\text{Te}_{0.9}\text{Se}_{0.1}$.

Fig.S15 High-temperature (300 K-673 K) stability of electrical conductivity and Seebeck coefficient in $(\text{AgCu})_{0.995}\text{Te}_{0.9}\text{Se}_{0.1}$.

Fig.S16 Temperature dependence of electrical conductivity and Seebeck coefficient on the repeat fabrication samples in $(\text{AgCu})_{0.995}\text{Te}_{0.9}\text{Se}_{0.1}$.

Fig.S17 Current dependence of output power, heat flow out of cold side, and conversion efficiency for a p-type $(\text{AgCu})_{0.995}\text{Te}_{0.9}\text{Se}_{0.1}$ single leg at different hot-side temperature.

Table S1 Room-temperature Hall carrier concentrations and densities for the $(\text{AgCu})_{1-x}\text{Te}_{0.9}\text{Se}_{0.1}$ ($x=-0.025, 0, 0.005, 0.01, 0.075$) samples.

Detailed descriptions and error analysis of thermoelectric conversion efficiency measurement

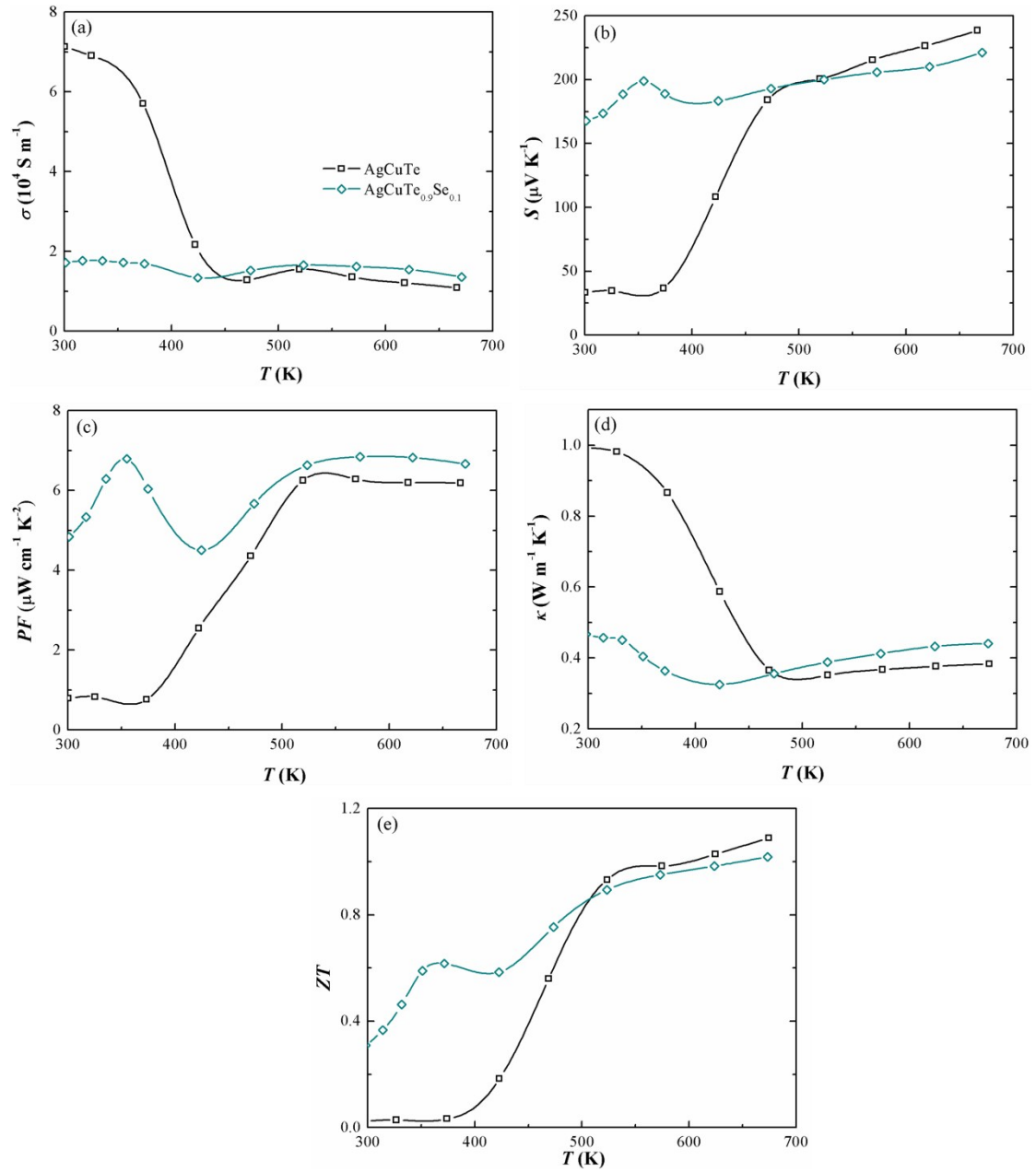


Fig.S1 Temperature dependence of thermoelectric properties for AgCuTe and AgCuTe_{0.9}Se_{0.1}. (a) Electrical conductivity (σ). (b) Seebeck coefficient (S). (c) Power factor (PF). (d) Total thermal conductivity (κ). (e) ZT values.

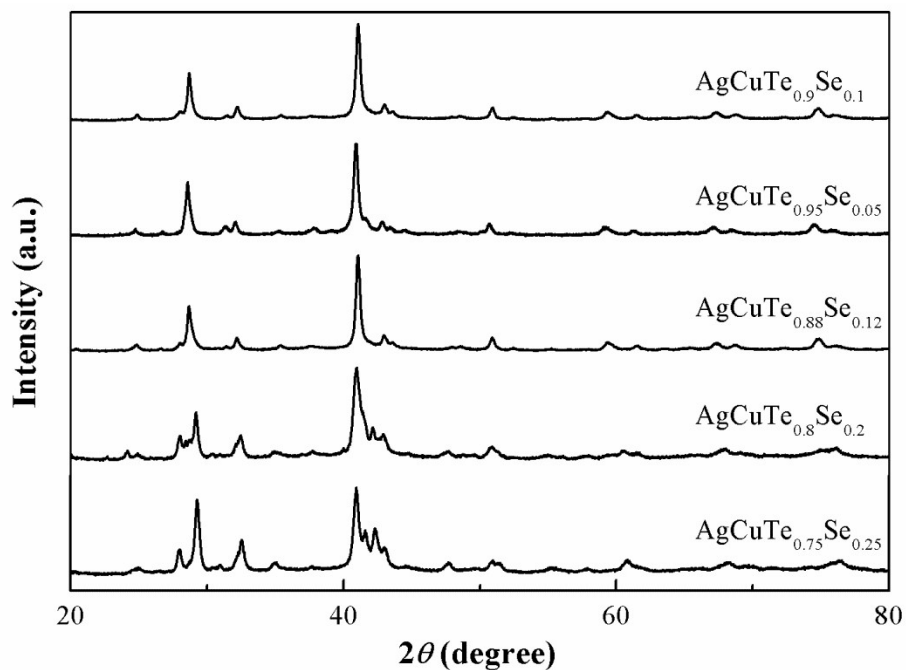


Fig.S2 Room-temperature XRD analyses for the $\text{AgCuTe}_{1-z}\text{Se}_z$ ($z=0.05, 0.1, 0.12, 0.2, 0.25$) samples. Increasing Se content to more than 20% deviates the main phase from the cubic phase.

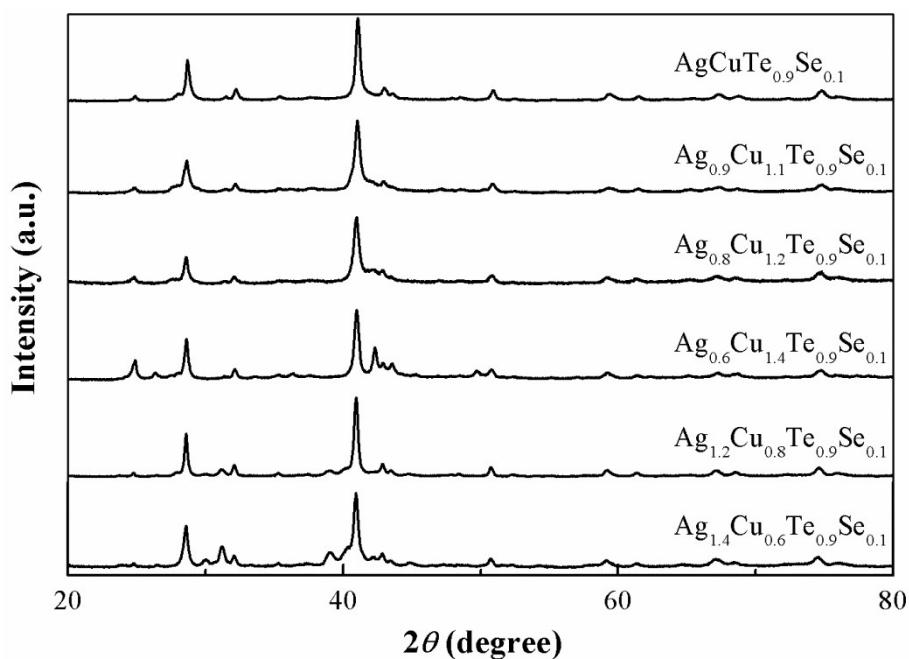


Fig.S3 Room-temperature XRD analyses for the $\text{Ag}_y\text{Cu}_{2-y}\text{Te}_{0.9}\text{Se}_{0.1}$ ($y=0.6, 0.8, 0.9, 1, 1.2, 1.4$) samples. Changing Ag/Cu ratio to away from 1:1 results in more impurity phases.

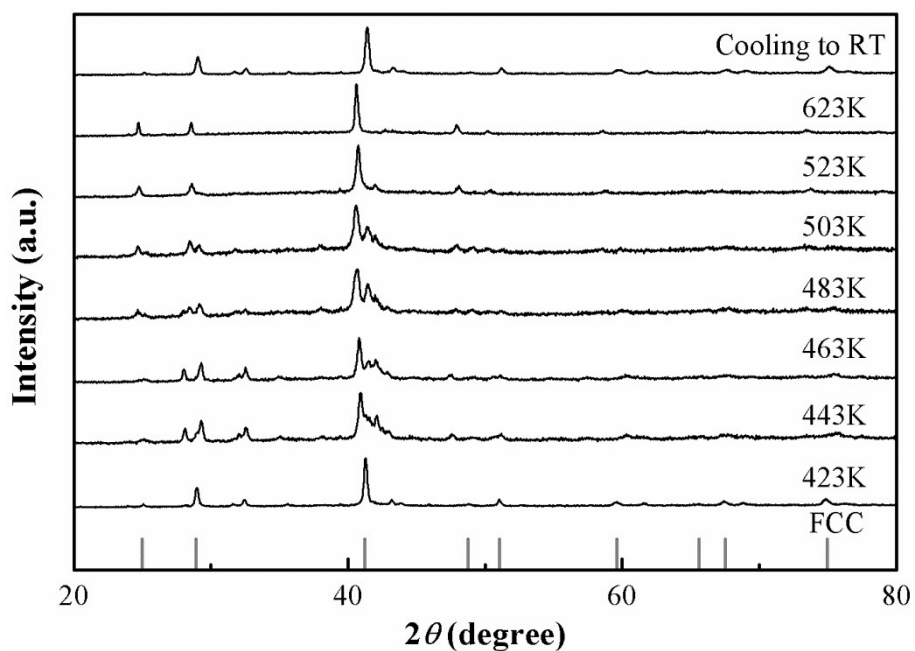


Fig.S4 Temperature-dependent XRD analyses for the $(\text{AgCu})_{0.995}\text{Te}_{0.9}\text{Se}_{0.1}$ sample. The measurement is conducted with increasing temperature. Every XRD pattern at different temperature is collected for about 1 hour. The XRD data is collected at room temperature again after the whole measurement for comparison. The FCC peak can always be observed over the measured temperature range. The impurity phases begin to dissolve into the main FCC phase with increasing temperature over 423 K, and no obvious impurity can be observed when temperature is as high as 623 K.

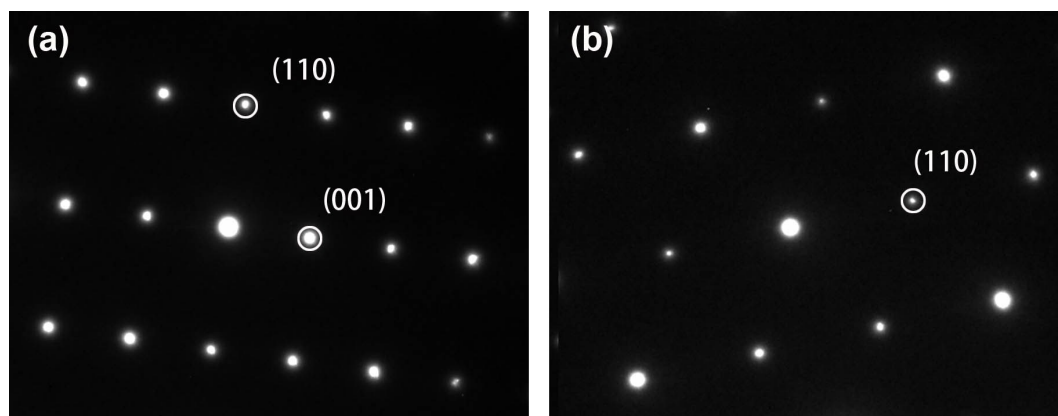


Fig.S5 The SAED pattern of the main phase with the electron beam along the direction of (a) $[1-10]$, and (b) $[111]$.

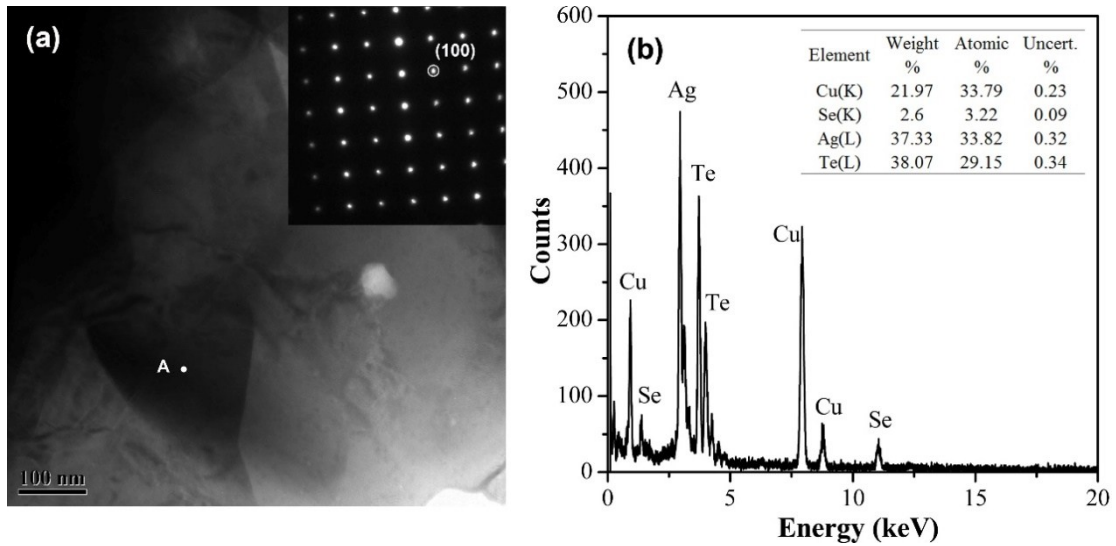


Fig.S6 Microstructure analyses of the FCC phase for the $\text{AgCuTe}_{0.9}\text{Se}_{0.1}$ sample. (a) The TEM image and SAED pattern recorded on the A point. The lattice parameter of 0.62 nm is calculated from the SAED pattern. (b) EDS results collected from the A point, which is similar with the nominal composition.

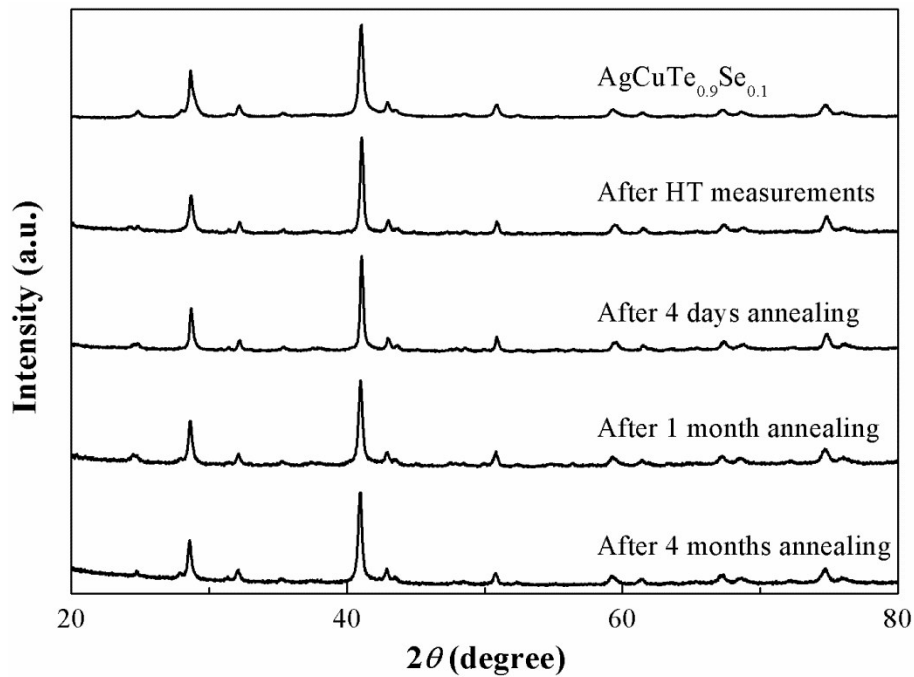


Fig.S7 Room-temperature XRD analyses for the $\text{AgCuTe}_{0.9}\text{Se}_{0.1}$ sample after high-temperature measurements and long-term annealing. The highest measurement temperature is 673K. The annealing is proceeded in the air at the temperature of about 360K for 4 days, 1month, and 4 months.

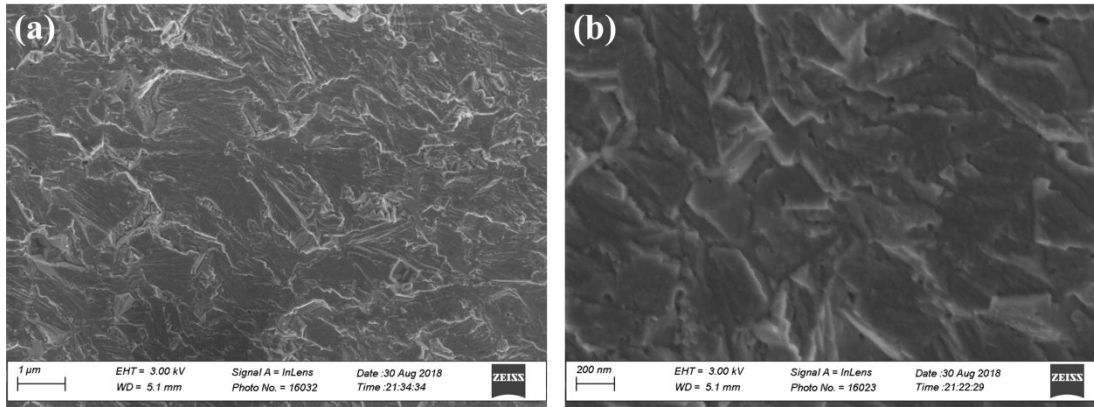


Fig.S8 Room-temperature SEM analyses for the $(\text{AgCu})_{0.995}\text{Te}_{0.9}\text{Se}_{0.1}$ sample with a hot-press temperature of 473K. The sample is tightly-condensed.

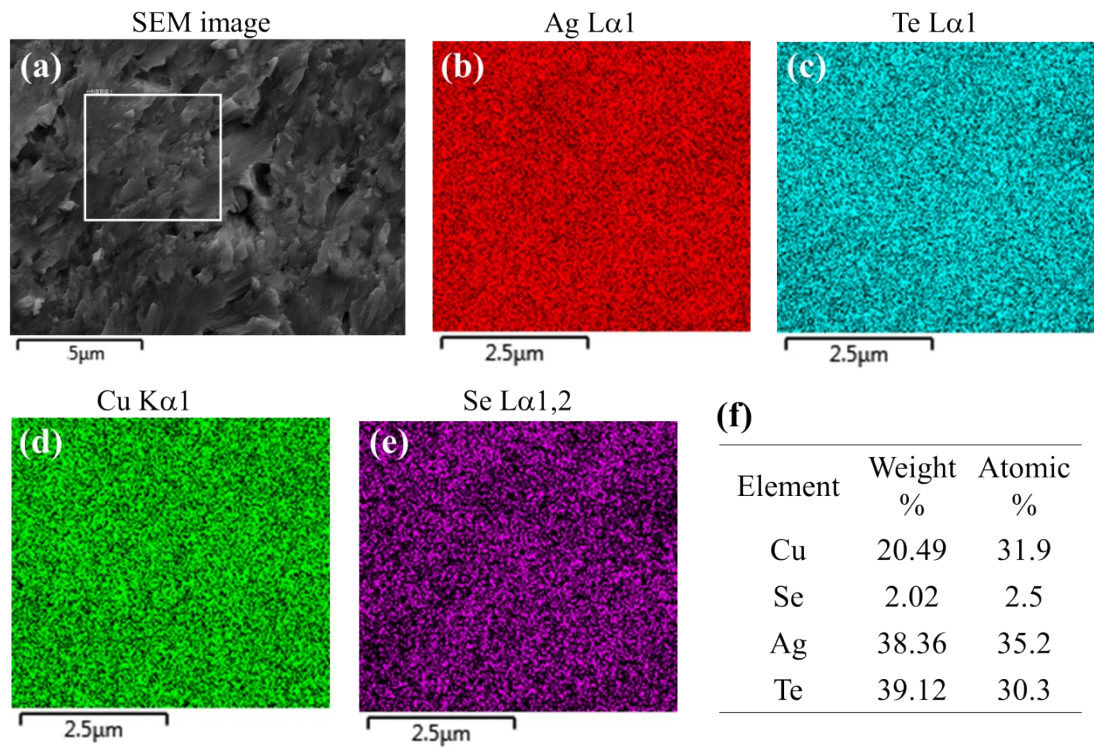


Fig.S9 Room-temperature SEM image with the EDS mapping for the $(\text{AgCu})_{0.995}\text{Te}_{0.9}\text{Se}_{0.1}$ sample with a hot-press temperature of 473K. (a) SEM image. The EDS mapping of element (b) Ag, (c) Te, (d) Cu, and (e) Se. (f) The composition results.

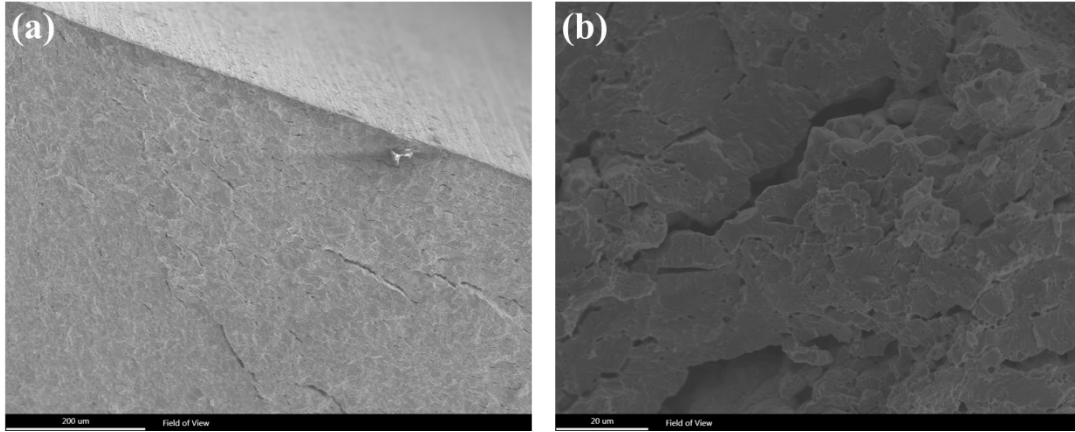


Fig.S10 Room-temperature SEM analyses for the $(\text{AgCu})_{0.995}\text{Te}_{0.9}\text{Se}_{0.1}$ sample with a hot-press temperature of 923K. The sample has a large number of cracks, which are orientated perpendicular to the hot-pressed direction.

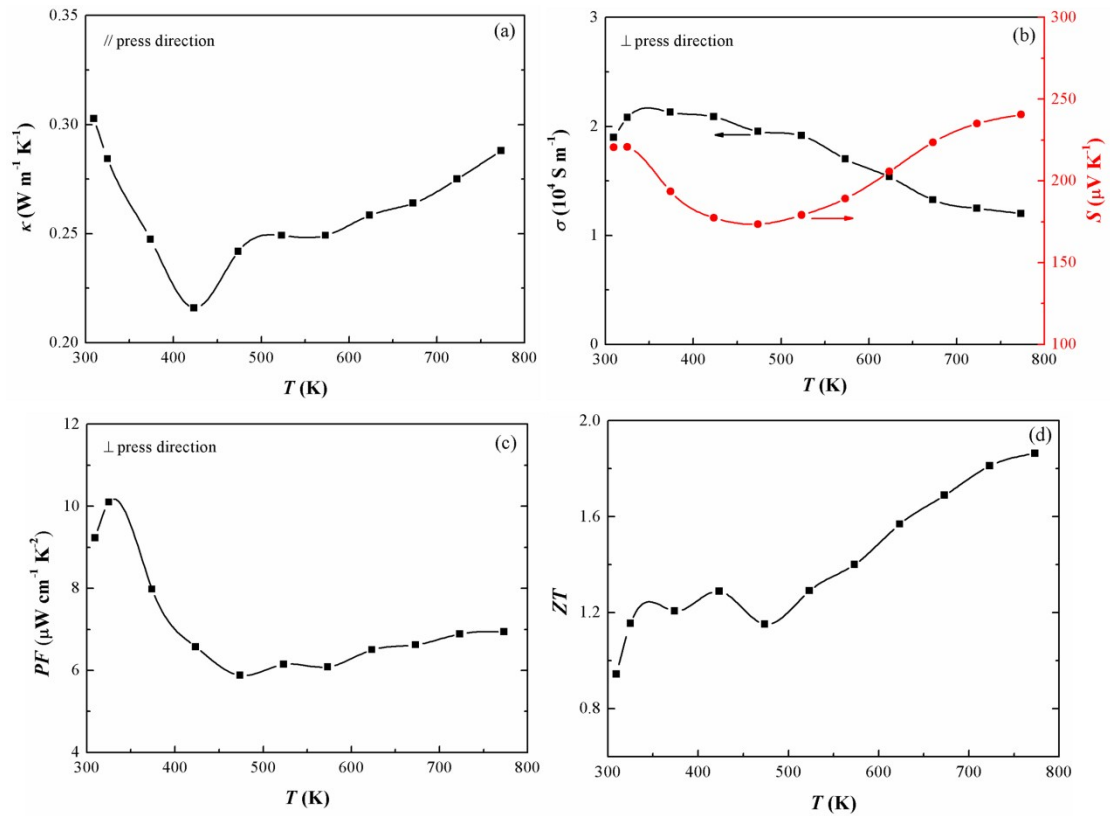


Fig.S11 Fake ultra-high ZT s for the $(\text{AgCu})_{0.995}\text{Te}_{0.9}\text{Se}_{0.1}$ sample with a hot-press temperature of 923K. Temperature dependence of (a) total thermal conductivity (κ) in the plane parallel to the press direction, (b) electrical conductivity (σ) and Seebeck coefficient (S) in the plane perpendicular to the press direction, (c) power factor (PF) in the plane perpendicular to the press direction, and (d) ZT values obtained by the combination of (a) and (c). The highly-orientated cracks lead to ultra-low thermal conductivities in the plane parallel to the press direction, while having little influence to the electrical properties in the plane perpendicular to the press direction. Fake ultra-high ZT s will be obtained by the combination of the thermal conductivity measured parallel to the hot-press direction and the electronic properties measured perpendicular to the hot-press direction.

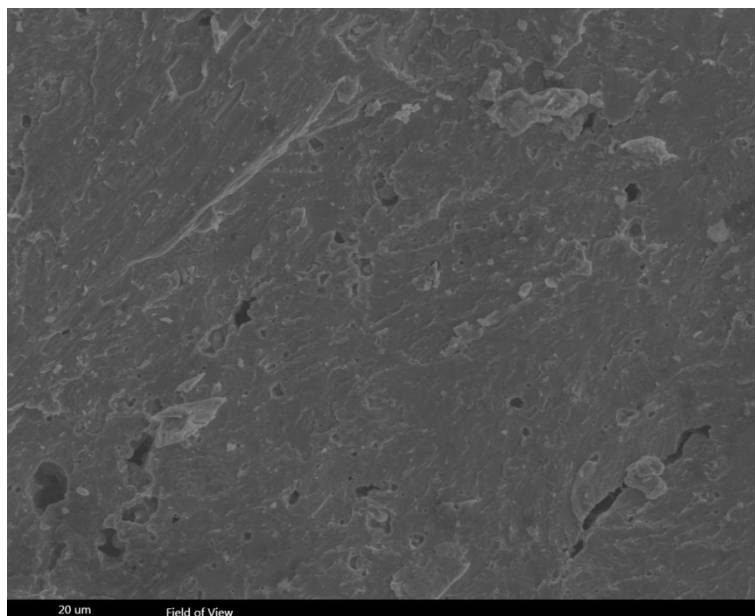


Fig.S12 Room-temperature SEM analysis for the $(\text{AgCu})_{0.995}\text{Te}_{0.9}\text{Se}_{0.1}$ sample with a hot-press temperature of 823K.

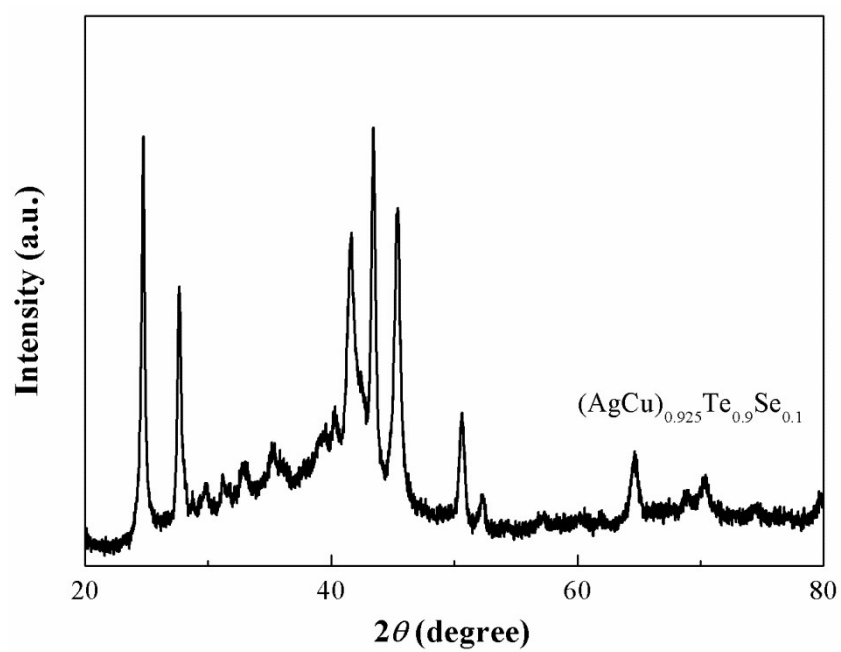


Fig.S13 Room-temperature XRD analysis for the $(\text{AgCu})_{0.925}\text{Te}_{0.9}\text{Se}_{0.1}$ sample. A large amount of impurity phases exist in this sample.

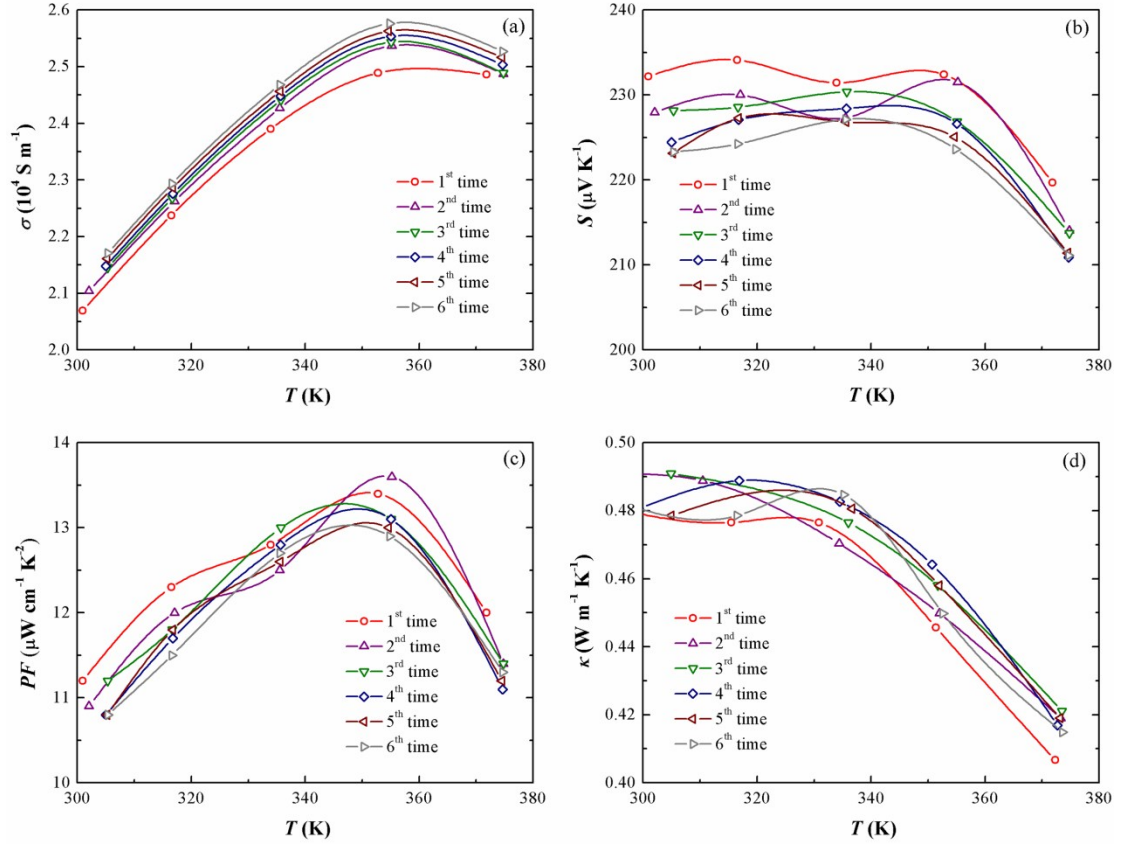


Fig.S14 Low-temperature stability of thermoelectric properties in $(\text{AgCu})_{0.995}\text{Te}_{0.9}\text{Se}_{0.1}$. Temperature dependence of (a) electrical conductivity (σ), (b) Seebeck coefficient (S), (c) power factor (PF), and (d) total thermal conductivity (κ) of one sample measured six times in the temperature range from 300K to 373K.

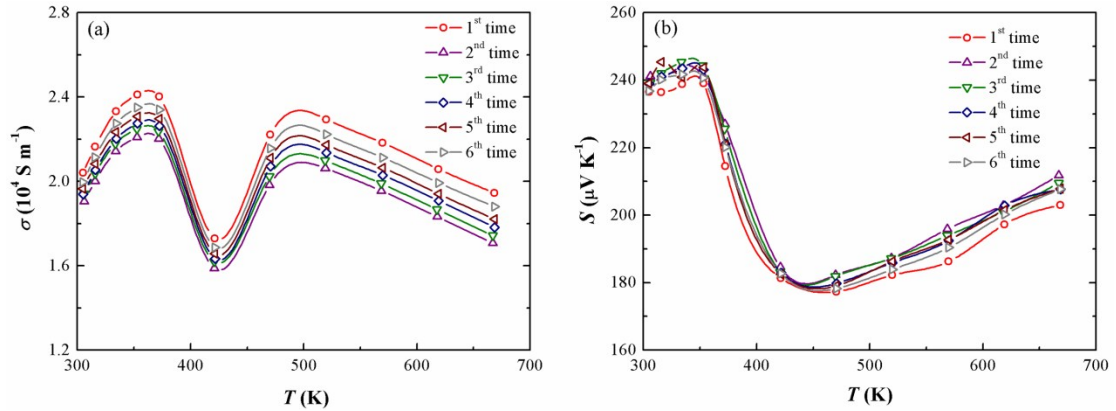


Fig.S15 High-temperature stability of (a) electrical conductivity (σ) and (b) Seebeck coefficient (S) of $(\text{AgCu})_{0.995}\text{Te}_{0.9}\text{Se}_{0.1}$ sample measured six times in the temperature range from 300K to 673K.

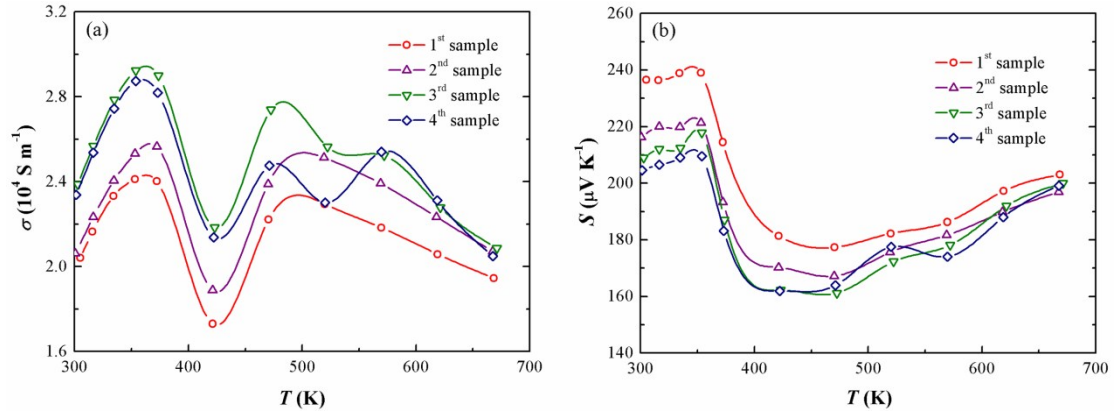


Fig.S16 Temperature dependence of (a) electrical conductivity (σ) and (b) Seebeck coefficient (S) of 4 batches of $(\text{AgCu})_{0.995}\text{Te}_{0.9}\text{Se}_{0.1}$ samples in the temperature range from 300K to 673K.

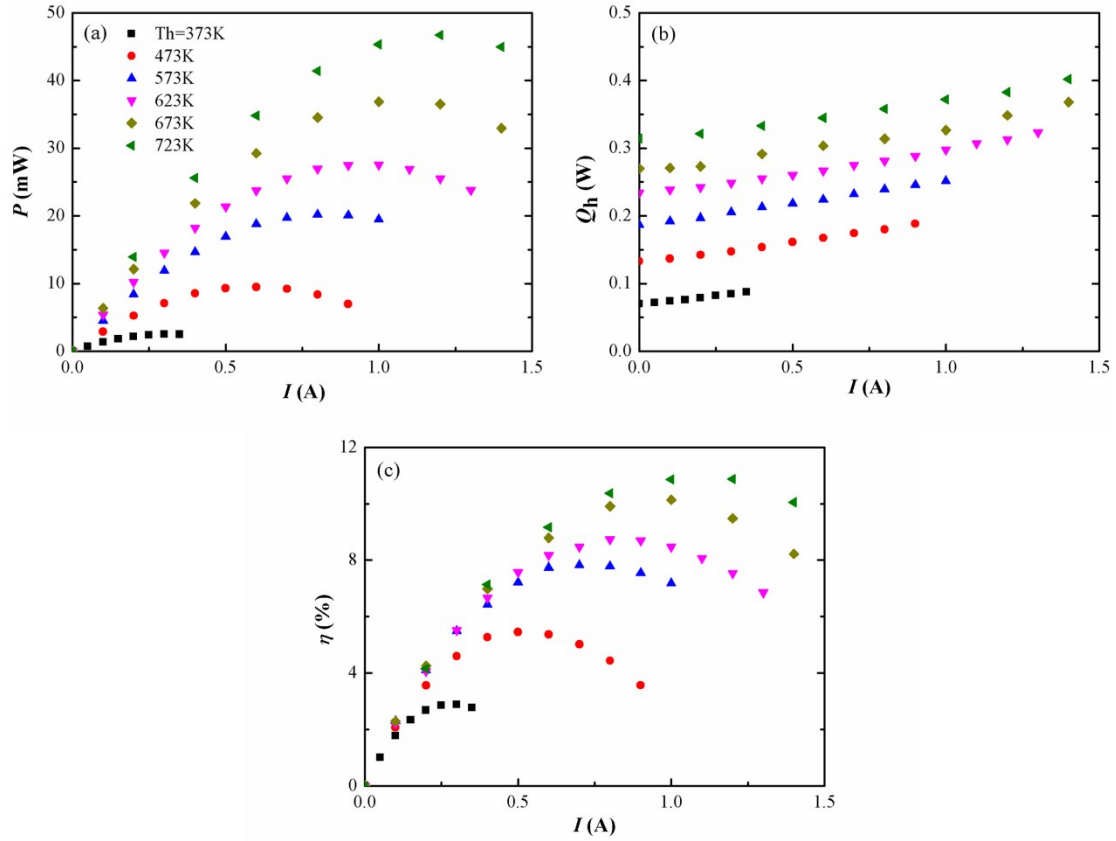


Fig.S17 Current dependence of (a) output power (P), (b) heat flow out of cold side (Q_h), and (c) conversion efficiency (η) for the p-type $(\text{AgCu})_{0.995}\text{Te}_{0.9}\text{Se}_{0.1}$ single leg at different hot-side temperature (T_h). By tuning the current I , the load impedance can be optimized and the maximum output power and conversion efficiency are obtained. The experimental values of output power and conversion efficiency shown in Fig. 5 are the maximum output power and conversion efficiency at different T_h , while that of thermal conductivity shown in Fig. 5 is calculated using the formula of $\kappa = Q_h / \Delta T S$, where Q_h is the heat flow at the optimal current, I , ΔT and S are defined in the section of efficiency measurement.

Table S1 Room-temperature Hall carrier concentrations and densities for the $(\text{AgCu})_{1-x}\text{Te}_{0.9}\text{Se}_{0.1}$ ($x=0.025, 0, 0.005, 0.01, 0.075$) samples.

Sample	Hall carrier concentration (cm^{-3})	Density (g cm^{-3})
$(\text{AgCu})_{1.025}\text{Te}_{0.9}\text{Se}_{0.1}$	-5.08×10^{19}	8.03
$\text{AgCuTe}_{0.9}\text{Se}_{0.1}$	-6.55×10^{19}	7.93
$(\text{AgCu})_{0.995}\text{Te}_{0.9}\text{Se}_{0.1}$	9.62×10^{19}	8.04
$(\text{AgCu})_{0.99}\text{Te}_{0.9}\text{Se}_{0.1}$	4.13×10^{20}	7.99
$(\text{AgCu})_{0.925}\text{Te}_{0.9}\text{Se}_{0.1}$	6.49×10^{21}	6.95

Detailed descriptions and error analysis of thermoelectric conversion efficiency measurement

The standard sample in Fig. 5(a) is used to measure the heat flow thus to calculate the thermal conductivity and thermoelectric conversion efficiency of the $(\text{AgCu})_{0.995}\text{Te}_{0.9}\text{Se}_{0.1}$ single leg. The cold side temperature of the standard sample (T_c') is almost fixed at 295 K by the cooling system, while the cold side temperature of the measured sample (T_c) changes from 298K to 322K with the increase of hot side temperature (T_h) from 373K to 723K. The heat flow out of cold side (Q_h) and the thermal conductivity of the measured sample (κ) are defined as:

$$Q_h = \kappa_s \Delta T_s S_s / l_s \quad (1)$$

$$\kappa = Q_h l / \Delta T S \quad (2)$$

Where κ_s is the thermal conductivity of the standard sample, ΔT_s and ΔT are the temperature difference on the standard sample and the measured sample respectively, defined as $\Delta T_s = T_c - T_c'$ and $\Delta T = T_h - T_c$. S_s and l_s are the sectional area and length of the standard sample respectively. S and l are the sectional area and length of the measured sample respectively.

The thermal conductivity of sample with the hot side temperature of T_h is actually an average thermal conductivity $(\kappa)_{\text{avg}}$ between T_c and T_h . The large difference between experimental and calculation thermal conductivities is caused by the experimental errors, which is a combined effect of the measurement errors of three thermocouples, the heat radiation of two samples and other thermal losses. The experimental error at low temperature is mainly caused by the thermocouple errors.

The thermal conductivity of Constantane is almost 40 times of that of $(\text{AgCu})_{0.995}\text{Te}_{0.9}\text{Se}_{0.1}$. Therefore the temperature difference on Constantane (ΔT_s) is about only 3K when T_h is as low as 373 K, leading to a thermocouple error of ± 0.2 K and a relative error of about 15% in the measured thermal conductivity. As the standard sample changing to Mg_3Sb_2 with much closer thermal conductivities (1-1.05 $\text{Wm}^{-1}\text{K}^{-1}$ at 300-400 K) to that of $(\text{AgCu})_{0.995}\text{Te}_{0.9}\text{Se}_{0.1}$ (0.4-0.45 $\text{Wm}^{-1}\text{K}^{-1}$ at 300-400 K), ΔT_s becomes larger so the relative error in experimental thermal conductivity becomes smaller. Therefore, the experimental thermal conductivities are very close to the calculation results by reducing the system error from the small heat flow, as shown by the blue triangles in Fig. 5(c).

The output power P and thermoelectric conversion efficiency η are defined as:

$$P = IV \quad (3)$$

$$\eta = P/(Q_h + P) \quad (4)$$

Where I and V are the current and voltage of the measured sample respectively.